

Journal Pre-proof

Direct imaging of pulmonary gas exchange with hyperpolarized xenon MRI

Haidong Li, Hongchuang Li, Ming Zhang, Chaolin Huang, Xin Zhou



PII: S2666-6758(24)00158-9

DOI: <https://doi.org/10.1016/j.xinn.2024.100720>

Reference: XINN 100720

To appear in: *The Innovation*

Received Date: 5 March 2024

Revised Date: 17 October 2024

Accepted Date: 17 October 2024

Please cite this article as: Li, H., Li, H., Zhang, M., Huang, C., Zhou, X., Direct imaging of pulmonary gas exchange with hyperpolarized xenon MRI, *The Innovation* (2024), doi: <https://doi.org/10.1016/j.xinn.2024.100720>.

This is a PDF file of an article that has undergone enhancements after acceptance, such as the addition of a cover page and metadata, and formatting for readability, but it is not yet the definitive version of record. This version will undergo additional copyediting, typesetting and review before it is published in its final form, but we are providing this version to give early visibility of the article. Please note that, during the production process, errors may be discovered which could affect the content, and all legal disclaimers that apply to the journal pertain.

© 2024 Published by Elsevier Inc. on behalf of Youth Innovation Co., Ltd.

Haidong Li,^{1,2,5} Hongchuang Li,^{1,2,5} Ming Zhang,^{1,2,5} Chaolin Huang,³ and Xin Zhou^{1,2,4,*}

¹State Key Laboratory of Magnetic Resonance and Atomic and Molecular Physics, Innovation Academy for Precision Measurement Science and Technology, Chinese Academy of Sciences, Wuhan 430071, China

²University of Chinese Academy of Sciences, Beijing 100049, China

³Jin Yin-tan Hospital, Wuhan 430048, China

⁴School of Biomedical Engineering, Hainan University, Haikou 570228, China

⁵These authors contributed equally

*Correspondence: xinzhou@wipm.ac.cn

Dear Editor,

Chronic respiratory diseases, including chronic obstructive pulmonary disease (COPD), interstitial lung disease (ILD), and asthma, are among the leading causes of morbidity and mortality worldwide. Recent estimates indicate that chronic respiratory diseases affect over 540 million people in the world in 2017 and account for an estimated 3.9 million deaths.¹ Medical imaging plays a pivotal role in the diagnosis, progression monitoring, treatment planning, and outcome evaluation of respiratory diseases. Despite the tremendous developments in medical imaging technology, currently no tools are available that could directly depict, quantify, and localize the gas exchange of oxygen from the alveoli to the lung parenchyma and blood.

Gas exchange is a critical function of the lung, yet it is not possible to non-invasively visualize this process with current clinical methods. Magnetic resonance imaging (MRI) using hyperpolarized noble gases ^3He and ^{129}Xe has facilitated the development of unique strategies for evaluating lung structure and gas exchange function.² In particular, the solubility of ^{129}Xe in biological tissues, combined with its sensitivity to the surrounding environment, makes hyperpolarized ^{129}Xe MRI uniquely capable of characterizing regional gas exchange,³ which is not accessible with the use of hyperpolarized ^3He . Hyperpolarized ^{129}Xe gas MRI has shown significant promise in detecting and evaluating abnormalities in pulmonary small airways, parenchyma, and vasculature by quantifying ventilation, gas diffusion, and regional gas exchange. This technique has been widely used to assess the microstructure and functional changes caused by lung diseases, such as COPD, ILD and COVID-19. Additionally, it has received clinical approval in both China and the United States.

Upon inhalation, xenon atoms enter the alveolar airspaces and diffuse through the pulmonary membrane (e.g., alveolar epithelial cells, interstitial tissues, capillary endothelial cells) to tissue/plasma (TP), and finally reach red blood cells (RBC), exhibiting different resonance frequencies when residing in the airspace (@ 0 ppm), TP (@ 197 ppm), and RBC (@ 217 ppm) compartments.⁴ These are referred to as gas-phase ^{129}Xe in the airspace and dissolved-phase ^{129}Xe in TP and RBC (Figure 1A). Gas and dissolved-phase xenon atoms are in dynamic equilibrium and continually exchange before being carried away in the bloodstream. Of note, the quantitative characteristics of xenon gas exchange and uptake within the lung are influenced by parameters of physiological

relevance, such as the thickness of the blood-gas barrier. Therefore, measurements capable of quantifying these characteristics offer valuable insights into the understanding of the functional status of healthy and diseased lung.

Separate imaging of ^{129}Xe dissolved in RBC and TP is required for regional assessment of gas exchange in the lung. However, this is particularly challenging because of the low signal intensity (1-2% of that in the airspace) and short T_2^* (~ 1 ms at 3.0 T and ~ 0.5 ms at 7.0 T) of ^{129}Xe in dissolved versus gas phase, and the similar chemical shift of ^{129}Xe dissolved in RBC and TP. Several methods have been developed for spatial and spectral imaging of dissolved ^{129}Xe in the lung, but the majority required complicated calculations and corrections to remove the gas signal contamination⁶ and correct the B_0 field. Of note, these methods required separate scans for gas and dissolved-phase ^{129}Xe imaging, and resulted in an averaged $\sim 10\%$ gas-phase contamination of the dissolved-phase ^{129}Xe images,⁶ hindering accurate quantification of ^{129}Xe gas exchange from alveoli to TP and RBC. Simultaneous acquisition of gas and dissolved-phase ^{129}Xe images as well as matched spatial resolution are required for precise evaluation of lung gas exchange function. This is because gas or dissolved-phase ^{129}Xe images alone do not allow differentiation between pathological changes in ventilation versus those in tissue microstructure or blood flow. Normalizing dissolved ^{129}Xe images to ^{129}Xe gas images acquired at the same time point provides unbiased evaluation of gas exchange that distinctly differs from commonly used measurements. Previous studies attempted to address this issue by using low acquisition bandwidth,⁷ but distinguishing ^{129}Xe signals in TP and RBC has remained challenging. ^{129}Xe chemical shift imaging (CSI)⁸ appears to simultaneously capture gas and dissolved-phase ^{129}Xe signals in the lung. However, the inherent limitations of this technique, such as low spatial resolution (typical voxel size for spectroscopic imaging: $6.5 \times 6.5 \times 20\text{-}25$ mm³), extremely long scan time, and the inability of regional evaluation of lung gas exchange function, have significantly restricted its widespread application.

In this work, we present a new approach capable of simultaneously imaging ^{129}Xe in lung airspace and either TP or RBC for direct visualization and evaluation of gas exchange in the lung. The proposed approach differs from previous methods in that: 1) the spatial resolution of the generated ^{129}Xe MR images is 5 to 50 times greater than ^{129}Xe CSI; 2) dissolved-phase ^{129}Xe MR signals in TP and RBC are separately excited and collected; 3) ^{129}Xe atoms in gas-phase (airspace) and dissolved-phase (RBC or TP) are simultaneously imaged in the same scan

without complicated correction or separation calculations, enabling the accurate assessment of regional gas-gas and gas-blood exchange.

We have successfully tackled some of the technical challenges of simultaneously imaging gas and dissolved phase ^{129}Xe in the lung. In particular, we designed highly selective radio frequency (RF) pulses using a Shinnar–Le Roux (SLR) algorithm⁹ to separately excite ^{129}Xe atoms dissolved in TP and RBC, and concomitantly acquire ^{129}Xe signals in lung airspace using a small flip angle by carefully adjusting the off-resonance effect of the pulse (Figure 1A). In addition, we developed a new data acquisition strategy enabling simultaneous spatial encoding of ^{129}Xe signals in RBC (or TP) and airspace in an interleaved manner (Figure 1A) based on 3D ultra-short echo time radial sampling. The acquired spokes are deployed in a temporally random order based on a Halton sequence, ensuring they are randomly and uniformly distributed throughout the sampling process. Furthermore, we proposed an image reconstruction strategy to separate the gas and dissolved-phase ^{129}Xe signals by modulating the phase of k-space to remove the chemical shift artifacts produced by center-out radial sampling. This operation is equivalent to shifting the analog-to-digital converter (ADC) center frequency, f_{ADC} , to the resonance frequency of either gas or dissolved-phase ^{129}Xe in separate acquisitions, coined “Reconstruction with Virtual Rescan (RVR)”. Finally, we successfully obtained isotropic resolution gas and dissolved-phase ^{129}Xe images in a single scan, as shown in the Figure 1A.

We first evaluated the feasibility of the proposed method for simultaneous gas and dissolved-phase ^{129}Xe imaging in a rat model with pulmonary fibrosis under the approval of the Institutional Review Board (APM22036T). Compared with the control rats ($N = 10$), we observed visibly heterogeneous signal intensities in both gas and dissolved-phase ^{129}Xe images (voxel size: $0.5 \times 0.5 \times 0.5 \text{ mm}^3$) in the fibrosis rats ($N = 10$) created using the bleomycin treatment (Figure 1B). We calculated the RBC/Gas, TP/Gas, and RBC/TP ratios to quantify gas exchange efficiency between alveolar airspace, TP, and RBC. We observed lower RBC/TP (0.30 ± 0.07 vs 0.53 ± 0.06 , $P < 0.001$) and RBC/Gas ($[1.72 \pm 0.46] \times 10^{-3}$ vs $[2.26 \pm 0.29] \times 10^{-3}$, $P = 0.008$) and higher TP/Gas ($[6.36 \pm 1.57] \times 10^{-3}$ vs $[4.62 \pm 0.43] \times 10^{-3}$, $P = 0.005$) in the fibrosis group compared to the control group (Figure 1C), which may be due to the reduced capillary density, blood volume, and/or increased septal thickness.

Moreover, we found that the RBC/Gas, TP/Gas, and RBC/TP ratios were strongly correlated with those provided by magnetic resonance spectroscopy (MRS) (Figures 1D-F). Meanwhile, pulmonary function tests (PFTs) and histological analysis were also performed on each rat for additional validation. We observed lower quasi-static lung compliance (C_{qs}) in the fibrosis group (0.32 ± 0.10 mL/cm H₂O) compared with the control group (0.73 ± 0.15 mL/cm H₂O) with a statistically significant difference ($P < 0.001$), as shown in the Figure 1G. Compared with the control rats, thickened alveolar wall and increased collagen deposition could be easily observed in Masson's trichrome stained lung sections from fibrosis rats (Figure 1H). Histological analysis showed that the septal thickness and the collagen fraction were 6.44 ± 0.38 μ m and $16 \% \pm 2 \%$ for the control group, respectively, and these measurements were increased to 14.01 ± 2.55 μ m and $32 \% \pm 5 \%$ for the fibrosis group ($P < 0.001$) (Figure 1I and 1J). Additionally, the RBC/TP ratios obtained with the proposed method were strongly correlated with histological measurements (Figure 1K) and PFTs (Figure 1L), suggesting that the proposed method is promising for assessing pulmonary injuries caused by lung disease. While both non-localized ¹²⁹Xe MRS and PFTs can non-invasively evaluate lung gas exchange function,¹⁰ these approaches rely on global measurements and fail to capture the regional nature of structural and functional abnormalities in lung fibrosis. Such regional information is invaluable for optimizing treatment plans and developing novel therapies, highlighting a significant limitation in the sensitivity of these methods to detect changes in gas-exchange efficiency. Although ¹²⁹Xe MRSI or CSI could provide regional evaluation of lung gas exchange, their spatial resolution and long scan time restrict widespread application.⁸ Histological analyses, although capable of directly visualizing and assessing local lung fibrotic changes are highly invasive and do not permit *in vivo* measurements of the entire lung. In contrast, the proposed approach allows for non-invasive visualization and quantification of local gas exchange function of the lung, suggesting its utility for widespread clinical application.

The clinical utility of our approach was demonstrated on 10 healthy volunteers (HV) and 17 discharged patients recovering from severe COVID-19, under the approval of the Institutional Review Board (APMH22005A). Figure 1M presents the original gas- and dissolved phase ¹²⁹Xe images of the lung (voxel size: $5.5 \times 5.5 \times 5.5$ mm³), along with the ratio maps of RBC/Gas, TP/Gas, and RBC/TP for a HV and a patient with COVID-19. Compared

with the HVs, the patients with COVID-19 exhibited a significantly decreased RBC/TP ratio (0.25 ± 0.05 vs. 0.45 ± 0.12 , $P < 0.001$). These changes may be attributed to interstitial thickening and perfusion deficits caused by inflammation and possible fibrosis due to COVID-19. Additionally, the RBC/TP ratio was strongly correlated with that obtained with MRS (Figure 1N). PFTs were also performed on each subject, revealing a significant difference ($P < 0.001$) between the two groups (forced vital capacity [FVC]: 4.68 ± 0.86 L for HV, 3.25 ± 0.66 L for COVID-19; diffusing capacity of the lungs for carbon monoxide [DL_{CO}]: 10.16 ± 1.61 mL/min/mm Hg for HV and 6.74 ± 1.30 mL/min/mm Hg for COVID-19). Furthermore, RBC/TP ratio measurements correlated with FVC and DL_{CO} provided by PFTs (Figure 1O and 1P), indicating the effectiveness of the proposed approach for quantifying lung gas exchange function.

In addition, the feasibility of the regional assessment of gas exchange function in the lung was demonstrated in a typical patient with COVID-19 (Figure 1Q). The images clearly show significant heterogeneity in the RBC/Gas, TP/Gas, and RBC/TP ratio maps, especially in the 40th and 50th slice. Furthermore, the averaged RBC/Gas, TP/Gas, and RBC/TP ratio changes along the anterior-posterior direction are also evident.

In conclusion, we proposed a way to directly and simultaneously image the 3D distribution of gas and dissolved-phase xenon in the lung for assessing regional gas exchange in the alveolar airspace, RBC, and TP. Our approach was capable of spatially and spectrally resolving signals of ¹²⁹Xe in the three compartments, and provided gas exchange function measurements highly consistent with ¹²⁹Xe MRS in both animal and human studies.

REFERENCES

1. Spencer, L.J., Degu, A., Kalkidan, H.A., et al. (2018). Global, regional, and national incidence, prevalence, and years lived with disability for 354 diseases and injuries for 195 countries and territories, 1990-2017: a systematic analysis for the Global Burden of Disease Study 2017. *Lancet* **392**(10159):1789-1858. DOI: 10.1016/s0140-6736(18)32279-7.
2. Rao, Q., Li, H., Zhou, Q., et al. (2024). Assessment of pulmonary physiological changes caused by aging, cigarette smoking, and COPD with hyperpolarized ^{129}Xe magnetic resonance. *Eur Radiol*. DOI: 10.1007/s00330-024-10800-w.
3. Li, H., Zhao, X., Wang, Y., et al. (2021). Damaged lung gas exchange function of discharged COVID-19 patients detected by hyperpolarized ^{129}Xe MRI. *Sci Adv* **7**(1):eabc8180. DOI: 10.1126/sciadv.abc8180.
4. Driehuys, B., Cofer, G.P., Pollaro, J., et al. (2006). Imaging alveolar-capillary gas transfer using hyperpolarized ^{129}Xe MRI. *Proc. Natl. Acad. Sci. U. S. A.* **103**(48):18278-18283. DOI: 10.1073/pnas.0608458103.
5. Qing, K., Ruppert, K., Jiang, Y., et al. (2014). Regional mapping of gas uptake by blood and tissue in the human lung using hyperpolarized xenon-129 MRI. *J. Magn. Reson. Imaging* **39**(2):346-359. DOI: 10.1002/jmri.24181.
6. Willmering, M.M., Cleveland, Z.I., Walkup, L.L., and Woods, J.C. (2021). Removal of off-resonance xenon gas artifacts in pulmonary gas-transfer MRI. *Magn. Reson. Med.* **86**(2):907-915. DOI: 10.1002/mrm.28737.
7. Mugler, J.P., 3rd, Altes, T.A., Ruset, I.C., et al. (2010). Simultaneous magnetic resonance imaging of ventilation distribution and gas uptake in the human lung using hyperpolarized xenon-129. *Proc. Natl. Acad. Sci. U. S. A.* **107**(50):21707-21712. DOI: 10.1073/pnas.1011912107.
8. Collier, G.J., Schulte, R.F., Rao, M., et al. (2023). Imaging gas-exchange lung function and brain tissue uptake of hyperpolarized ^{129}Xe using sampling density-weighted MRSI. *Magn. Reson. Med.* **89**(6):2217-2226. DOI: 10.1002/mrm.29602.

9. Pauly, J., Le Roux, P., Nishimura, D., and Macovski, A. (1991). Parameter relations for the Shinnar-Le Roux selective excitation pulse design algorithm. *IEEE Trans. Med. Imaging* **10**(1):53-65. DOI: 10.1109/42.75611.
10. Kaushik, S.S., Freeman, M.S., Yoon, S.W., et al. (2014). Measuring diffusion limitation with a perfusion-limited gas--hyperpolarized ^{129}Xe gas-transfer spectroscopy in patients with idiopathic pulmonary fibrosis. *J Appl Physiol* **117**(6):577-585. DOI: 10.1152/jappphysiol.00326.2014.

ACKNOWLEDGMENTS.

This work is supported by National key Research and Development Program of China (grant no. 2022YFC2410000), National Natural Science Foundation of China (grant no. 82127802, 21921004, 82372150, 81930049, 82202119), the Strategic Priority Research Program of the Chinese Academy of Sciences (grant No. XDB0540000), Key Research Program of Frontier Sciences, CAS (grant no. ZDBS-LY-JSC004), Hubei Provincial Key Technology Foundation of China (2021ACA013), Major Program (JD) of Hubei Province (2023BAA021) and Hubei Provincial Outstanding Youth Fund (2023AFA112). Haidong Li acknowledges the support from Youth Innovation Promotion Association, CAS (grant no. 2020330).

DECLARATION OF INTERESTS

The authors declared no competing interest.

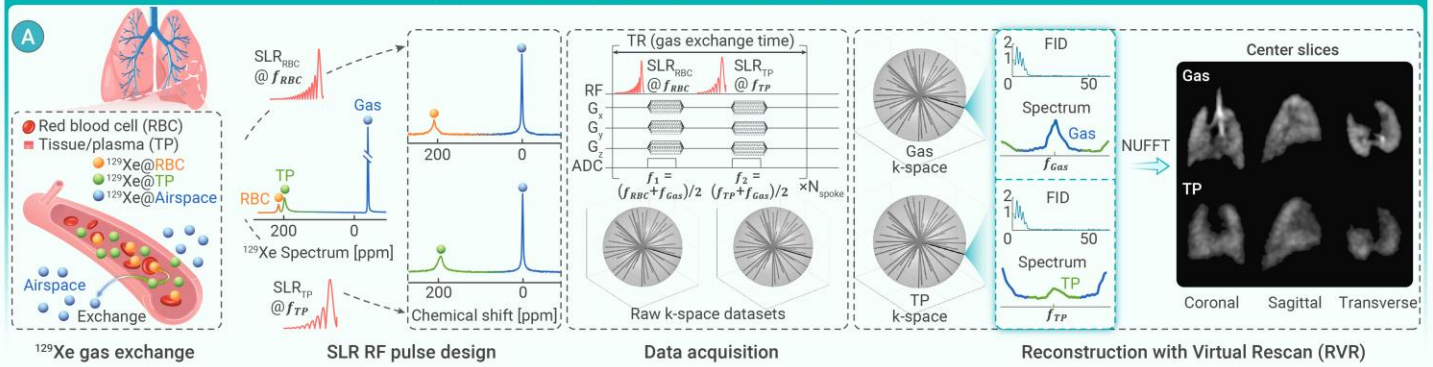
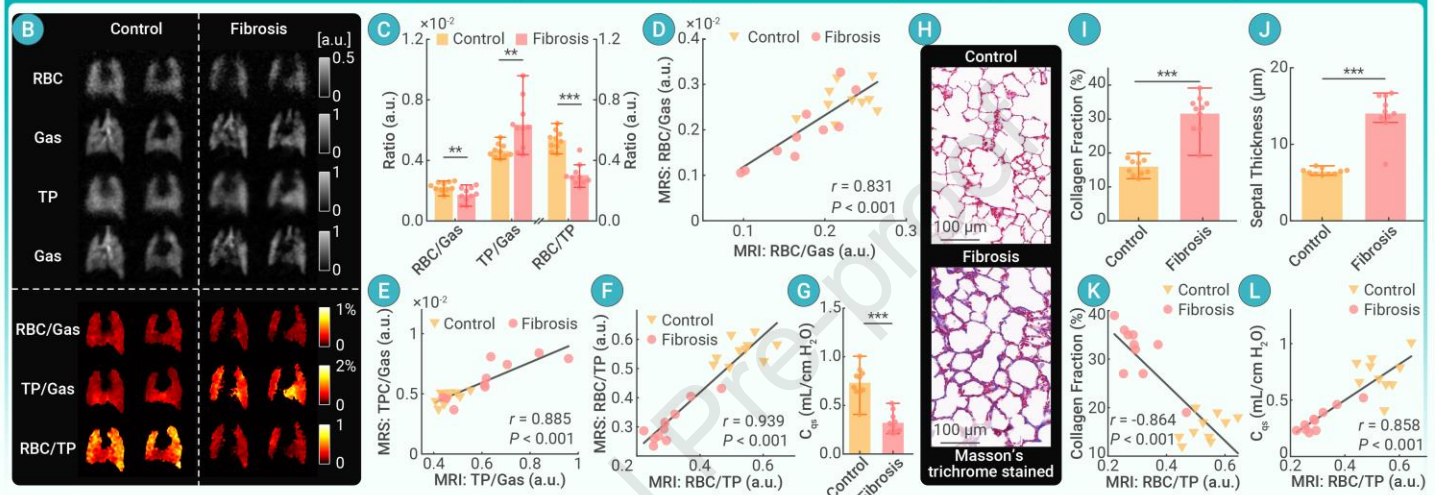
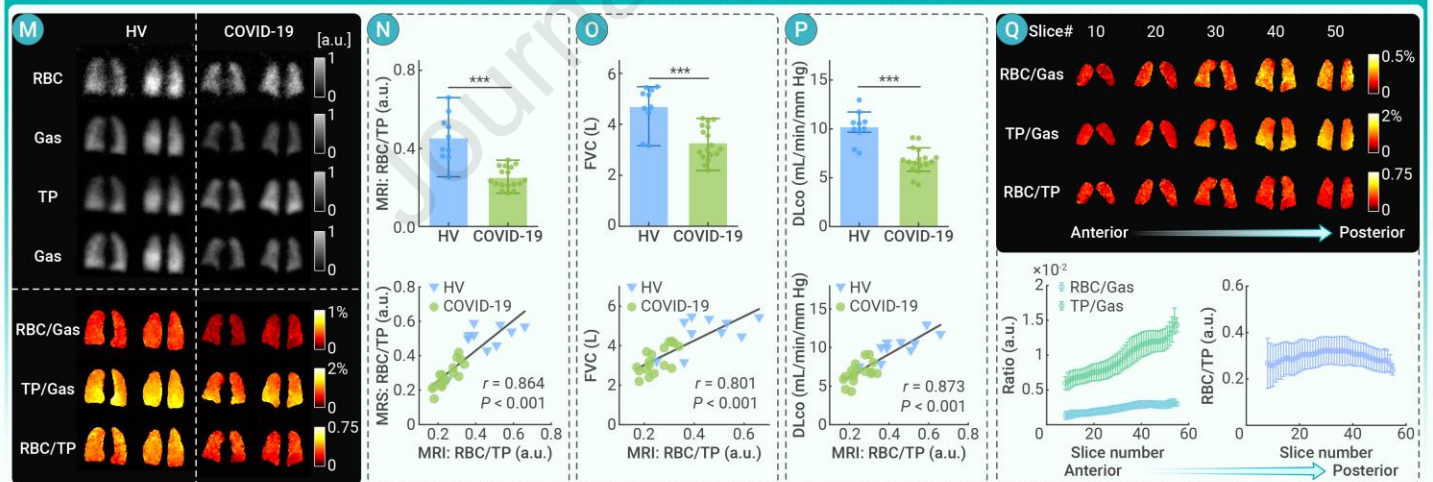
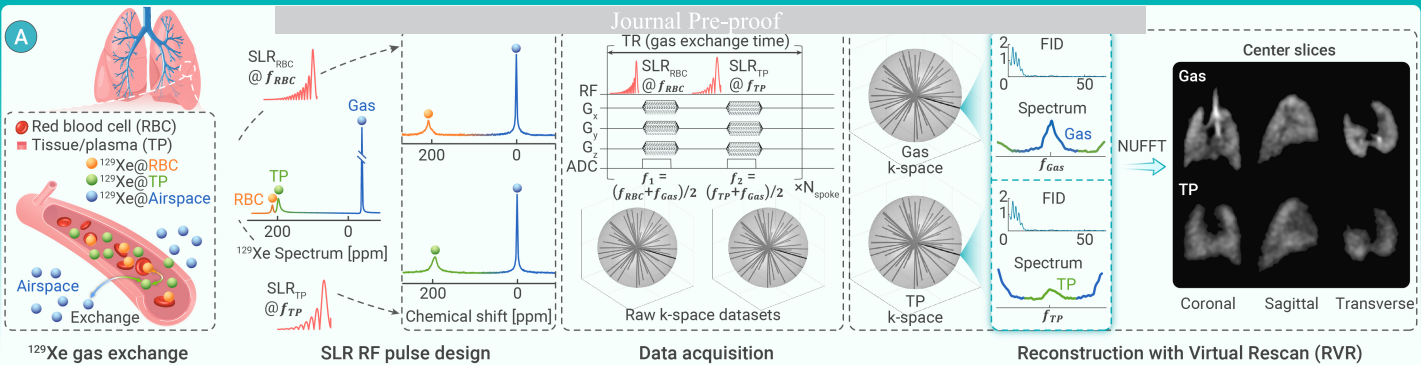
Schematic of simultaneous gas and dissolved-phase ^{129}Xe lung imagingResults of ^{129}Xe MRI, pulmonary function tests (PFTs), and histological analysis in the animal studyResults of ^{129}Xe MRI and PFTs in the human study

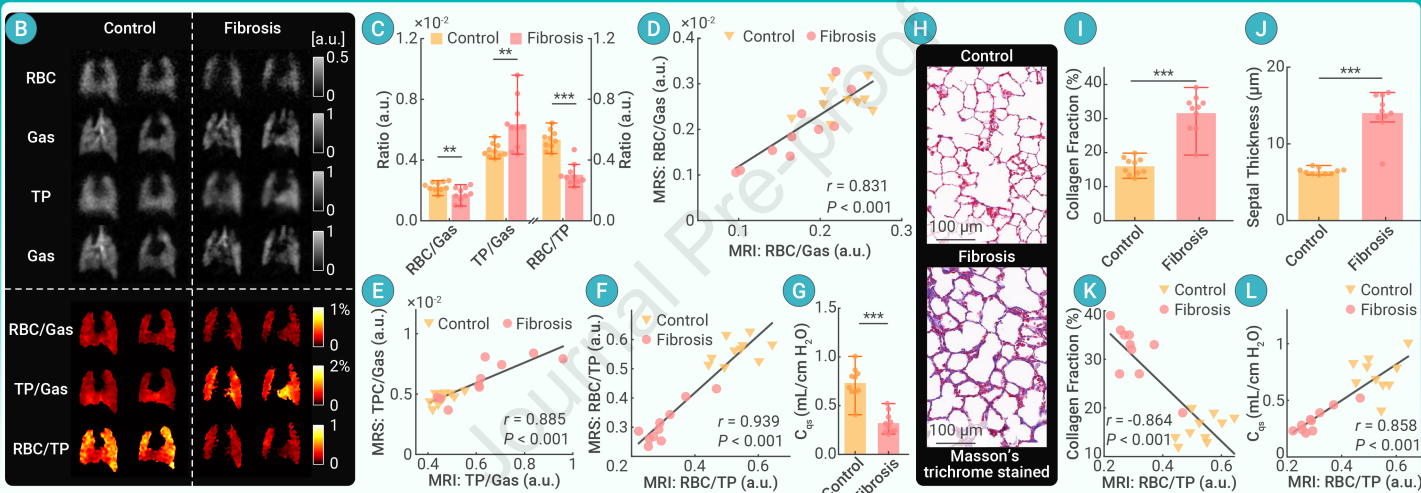
Figure 1. Simultaneous imaging of gas and dissolved-phase ^{129}Xe in the animal and human lung (A) Schematic of simultaneous gas and dissolved-phase ^{129}Xe lung imaging: *In vivo* measurements of ^{129}Xe MR signals in airspace and either RBC or TP using radio frequency (RF) pulses with high selectivity (SLR_{RBC} and SLR_{TP}); Diagram of the pulse sequences and data acquisition strategy for simultaneous gas and dissolved-phase

¹²⁹Xe imaging; Workflow for gas and dissolved-phase (using ¹²⁹Xe signal in TP as an example) ¹²⁹Xe image reconstruction using the Reconstruction with Virtual Rescan (RVR) method. (B) Representative images of ¹²⁹Xe MR signal in airspace, RBC, and TP, and ratio maps for a control and a fibrosis rat. (C) Comparison of group averaged RBC/Gas, TP/Gas, and RBC/TP ratios obtained from ¹²⁹Xe MRI between control and fibrosis rats. (D, E, and F) Correlations between averaged RBC/Gas, TP/Gas, and RBC/TP ratios obtained from ¹²⁹Xe MRI and magnetic resonance spectroscopy (MRS). (G) Comparison of group averaged quasi-static lung compliance (C_{qs}) measured by PFTs between the groups. (H) Typical Masson's trichrome stained images obtained from a control and a fibrosis rat, scale bar: 100 μ m. (I and J) Comparison of group averaged collagen fraction and septal thickness between the groups. (K and L) Correlations between the averaged RBC/TP ratio provided by ¹²⁹Xe MRI with collagen fraction and C_{qs} . (M) Representative images of ¹²⁹Xe MR signal in airspace, RBC, and TP, and ratio maps for a healthy volunteer (HV) and a discharged patient with COVID-19 (COVID-19). (N) Comparison of group averaged RBC/TP ratios obtained from ¹²⁹Xe MRI between the groups, and the correlation between the RBC/TP ratio obtained from ¹²⁹Xe MRI and whole lung MRS. (O) Comparison of group averaged forced vital capacity (FVC) between the groups and the correlation between the RBC/TP ratio obtained from ¹²⁹Xe MRI and FVC. (P) Comparison of group averaged DL_{CO} between the groups, and the correlation between the RBC/TP ratio obtained from ¹²⁹Xe MRI and DL_{CO} . (Q) The typical slices of RBC/Gas, TP/Gas, and RBC/TP maps, as well as the averaged RBC/Gas, TP/Gas, and RBC/TP ratio changes along the anterior-posterior direction from a patient with COVID-19. All the data are presented as mean \pm SD, and unpaired two-tailed t-tests and two-tailed Pearson correlation analyses were used. ** $P < 0.01$, *** $P < 0.001$.

Schematic of simultaneous gas and dissolved-phase ^{129}Xe lung imaging



Results of ^{129}Xe MRI, pulmonary function tests (PFTs), and histological analysis in the animal study



Results of ^{129}Xe MRI and PFTs in the human study

